

Atomistic Measures of Materials Strength

Ju Li¹, Sidney Yip¹

Abstract: We examine the role of atomistic simulations in multiscale modeling of mechanical behavior of stressed solids. Theoretical strength is defined through modes of structural instability which, in the long wavelength limit, are specified by criteria involving elastic stiffness coefficients and the applied stress; more generally, strength can be characterized by the onset of soft vibrational modes in the deformed lattice. Alternatively, MD simulation of stress-strain response provides a direct measure of the effects of small-scale microstructure on strength, as illustrated by results on SiC in single crystal, amorphous, and nanocrystalline phases. A Hall-Petch type scaling is introduced to estimate strength of laboratory specimens containing microstructural flaws of certain critical size. A preliminary simulation of Cu thin film nano-indentation is described as a means of probing the ideal shear strength. The challenge of formulating a local measure of the driving force for defect motion is briefly discussed.

1 Introduction

Currently there is widespread interest in identifying fundamental problems in materials modeling which combine scientific challenges with technologically relevant applications [Report of the National Workshop on Advanced Scientific Computing (1998)]. To provide a basis for such inquiries, we examine here a particular focus on the atomic-level understanding of mechanical behavior, in the context of a multiscale approach to materials theory and simulation [Special Issue of *J. Computer-Aided Mater. Design* (1996); Special issue of *Current Opinion in Solid State and Mater. Sci* (1998); Campbell, Foiles, Huang, Hughes, King, Lassila, Nikkel, de la Rubia, Shu and Smyshlyaev (1998)]. Our aim is to discuss how strength and deformation at the atomistic level can be probed through structural instability and modes of dynamical response to critical loading, with a view to-

ward linking the microscopic mechanisms to predictive mesoscale descriptions.

2 Atomistics of Strength and Deformation

The theoretical basis for describing the mechanical stability of a crystal lattice lies in the formulation of stability conditions which specify the critical level of external stress that the system can withstand. Lattice stability is not only one of the most central issues in elasticity, it is also fundamental in any analysis of structural transformations in solids, such as polymorphism, amorphization, fracture or melting. It was first shown by M. Born that by expanding the internal energy of a crystal in a power series in the strain and requiring positivity of the strain energy, one obtains a set of conditions on the elastic constants of the crystal that must be satisfied to maintain structural stability [Born (1940); Born and Huang (1956)]. This leads to the determination of ideal strength of perfect crystals as an instability phenomenon, a concept that has been examined by Hill (1975) and Hill and Milstein (1977), as well as used in various applications [Kelly and MacMillan (1986)]. That Born's results are valid only when the lattice is not under external stress was brought out explicitly in a derivation by Wang *et al* (1995) invoking the formulation of a path-dependent Gibbs integral. The limitation is most displayed by considering the relation between two second-rank tensors, the elastic stiffness coefficients \mathbf{B} and the elastic constants \mathbf{C} [Wallace (1972)],

$$B_{ijkl} = C_{ijkl} + \Lambda_{ijkl}, \quad (1)$$

where

$$\Lambda_{ijkl} = \frac{1}{2}(\delta_{ik}\tau_{jl} + \delta_{jk}\tau_{il} + \delta_{il}\tau_{jk} + \delta_{jl}\tau_{ik} - 2\delta_{kl}\tau_{ij}), \quad (2)$$

with δ_{ij} being the Kronecker delta symbol and τ_{ij} being the applied stress tensor. The condition for the onset of lattice instability is [Wang, Li, Yip, Phillpot, Wolf (1995)]

$$\det|\mathbf{A}| = 0, \quad (3)$$

¹Department of Nuclear Engineering, Massachusetts Institute of Technology, Cambridge, MA 02139, USA

where

$$A_{ijkl} = \frac{1}{2} (B_{ijkl} + B_{klij}). \quad (4)$$

In the absence of an external stress the elastic stiffness coefficients are the same as the elastic constants, in which case Eq.(3) gives the Born criteria. Conversely, at finite external stress lattice stability, or strength, is in principle not an intrinsic material property as are the elastic constants. In the derivation of Eq.(3) [Wang, Li, Yip, Phillpot, Wolf (1995)] the origin of the term Λ_{ijkl} arises clearly from the work done by the external stress. Further discussions of Eq.(3) has been given by Zhou and Joos (1996) regarding thermodynamic (ensemble) implications and the deformation path, and by Morris and Krenn (2000) regarding compatibility with the condition for internal stability formulated by Gibbs in 1876.

The connection between stability criteria and theoretical strength is rather straightforward. For a given applied stress one can imagine evaluating the current elastic constants to obtain the stiffness coefficients \mathbf{B} . Then by increasing the magnitude of stress one will reach a point where one of the eigenvalues of the matrix \mathbf{A} (cf. Eq.(3)) vanishes. This critical stress at which the system becomes structurally unstable is then a measure of the theoretical strength of the solid. In view of this, one has a direct approach to strength determination through atomistic simulation of the structural instability under a prescribed loading. If the simulation is performed by molecular dynamics, temperature effects can be taken into account naturally by following the particle trajectories at the temperature of interest.

Under a uniform load the deformation of a single crystal is homogeneous up to the point of structural instability. For a cubic lattice under an applied hydrostatic stress, the load-dependent stability conditions are particularly simple, being of the form,

$$C_{11} + 2C_{12} + P > 0, \quad C_{11} - C_{12} - 2P > 0, \quad C_{44} - P > 0, \quad (5)$$

where P is positive (negative) for compression (tension), and the elastic constants C_{ij} are to be evaluated at the current state. While this result is known for some time [Barron and Klein (1965); Hoover, Holt, Squire (1969); Basinski, Duesbery, Pogany, Taylor, Varshni (1970)] , direct verification against atomistic simulations showing that the criteria do accurately describe the critical value

of P_c at which the homogeneous lattice becomes unstable has been relatively recent [Wang, Li, Yip, Phillpot, Wolf (1995); Wang, Yip, Phillpot, Wolf (1993); Mizushima, Yip, Kaxiras (1994); Tang and Yip (1994); Cleri, Wang, Yip (1995); Tang and Yip (1995)]. One may therefore regard P_c as a definition of the theoretical or ideal compressive (tensile) strength of the lattice.

One may regard the stability criteria, Eq.(5), as manifestation in the long wavelength limit of the general condition for vibrational stability of a lattice. The vanishing of elastic stiffness then corresponds to the phenomenon of soft phonon modes in lattice dynamics. Indeed one finds that under sufficient deformation such soft modes do occur in a homogeneously strained lattice. In this work we will discuss molecular dynamics simulation results for cubic SiC (3C or β -phase) which has zinc-blende structure, obtained using an empirical bond-order potential [Tersoff (1989)]. For a specified deformation at constant strain, a single crystal sample with periodic boundary condition is relaxed at essentially zero temperature. The resulting atomic configurations are then used to construct and diagonalize the dynamical matrix. Fig. 1 shows two sets of dispersion curves, obtained at strain values close to critical for deformation under hydrostatic tension and shear respectively [Li (2000); Romano, Li, Yip (2002)]. Case (a) shows the Γ -point zone center soft mode in the [111] direction at a hydrostatic strain of 0.24 and stress of 39 GPa, which corresponds to an elastic instability, while case (b) shows the L-point zone boundary soft mode at a shear strain of 0.20 and a shear stress of 62 GPa, which is *not* an elastic instability. The implication here is that lattice vibrational analysis of a deformed crystal offers the most general measure of structural instability at zero temperature.

Returning to molecular dynamics simulations we show in Fig. 2 the stress-strain response for SiC under hydrostatic tension at 300K. At every step of fixed strain, the system is relaxed and the Virial stress evaluated. Three samples are studied with periodic boundary conditions, a single crystal (3C), an amorphous system that is a multiplication of a smaller configuration produced by electronic-structure calculations [Galli (1999)], and a nanocrystal composed of four distinct grains with random orientations (7,810 atoms). The single-crystal sample shows the expected linear elastic response at small strain up to about 0.03; thereafter the response is nonlinear but still elastic up to a critical strain of 0.155 and corresponding

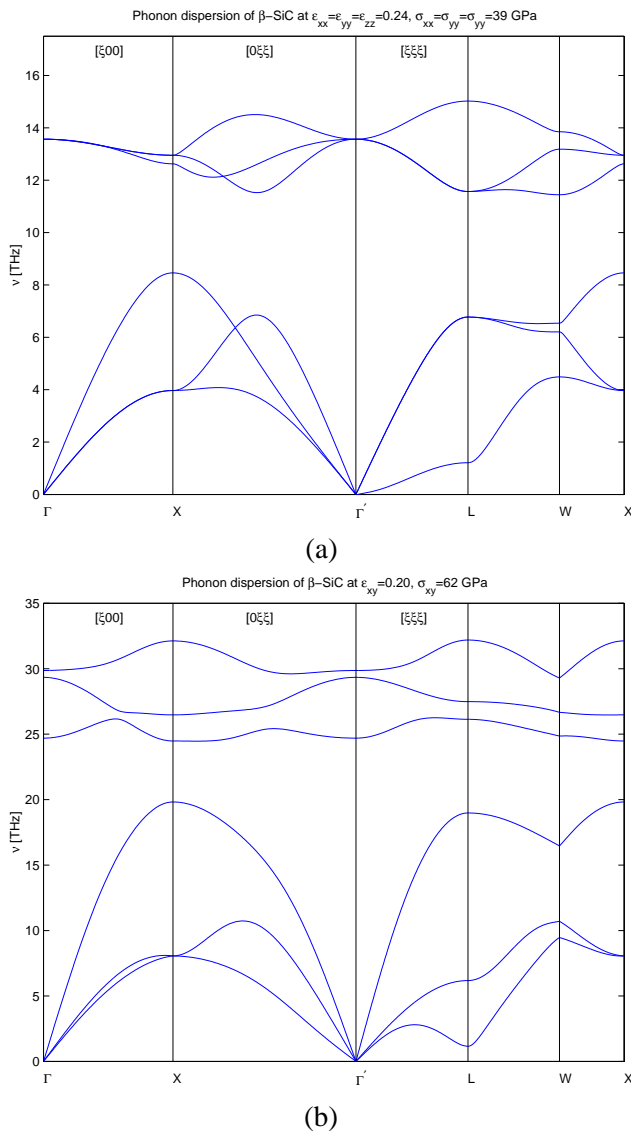


Figure 1 : Phonon dispersion curves of SiC (3C) at large strains, (a) hydrostatic tension, and (b) pure shear (same \mathbf{k} -point labeling but which only tracks one split branch of the original cubic-symmetry \mathbf{k} -point.).

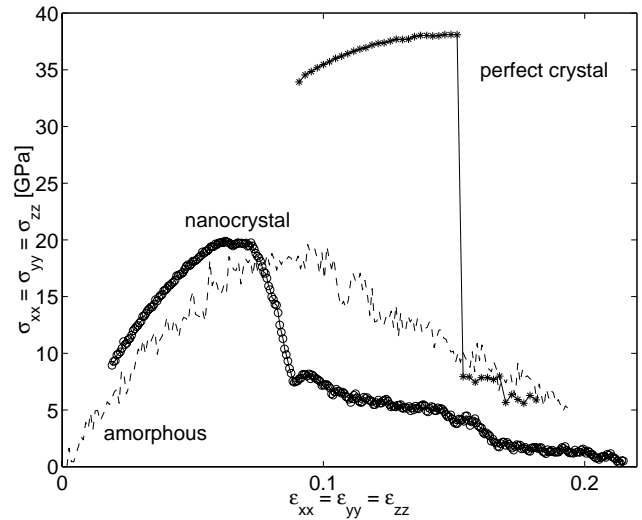
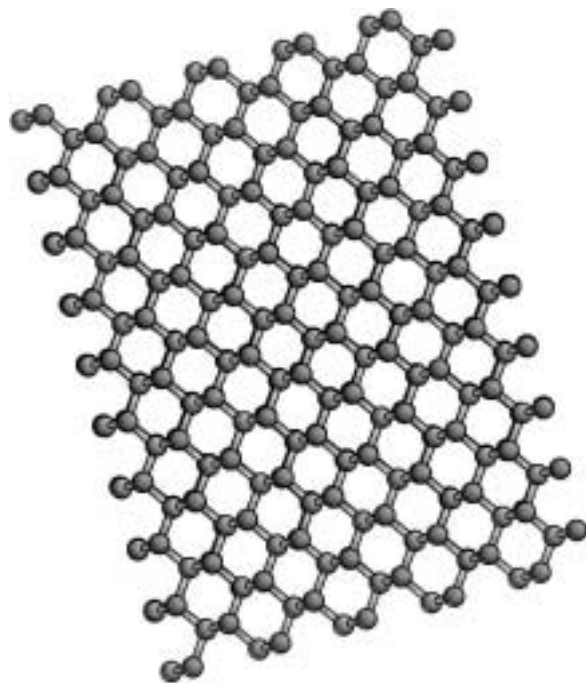


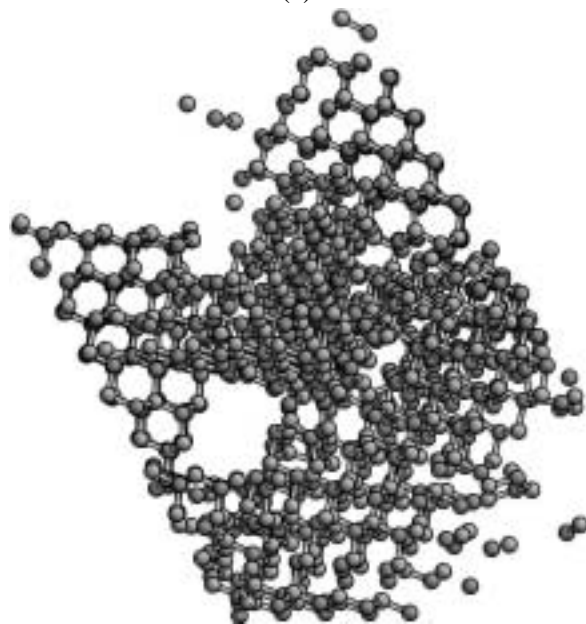
Figure 2 : Variation of Virial stress at constant strain from MD simulations of SiC (3C) under hydrostatic tension at 300K in perfect crystal, amorphous, and nanocrystalline phases.

stress of 38 GPa. Applying a small increment strain beyond this point causes a dramatic change with the internal stress suddenly reduced by a factor of 4. Inspection of the atomic configurations, Fig. 3, shows that the crystal has failed by spontaneous nucleation of microcracks.

The response curves for the amorphous and nanocrystal in Fig. 2 differ significantly from that of the single crystal, with interesting similarities and differences relative to each other. The former shows a broad peak, at about half the critical strain and stress of the perfect crystal, suggesting a much more gradual structural transition. Indeed, the atomic configuration, Fig. 4, shows fracture-like decohesion at strain of 0.096 and stress of 22 GPa. Another feature of the amorphous sample is that the instability under other modes of deformation, uniaxial tension and shear, occur at approximately the same stress (uniaxial tension: 25 GPa; shear: 19 GPa). This feature of *modal insensitivity* is in contrast to the perfect crystal results, failure stresses of 75 and 60 GPa for uniaxial tension and shear respectively while 38 GPa for hydrostatic tension, showing pronounced sensitivity. For the nanocrystal, the critical strain and stress are seen to be similar to the amorphous phase, except that the instability or failure effect is much more pronounced, qualitatively like that of the single crystal. The atomic configuration, Fig. 5, shows rather clearly the failure process



(a)



(b)

Figure 3 : Atomic configurations of a single crystal of SiC (3C) just prior to (a) and after (b) structural instability under hydrostatic loading at 300 K (see Fig. 2).

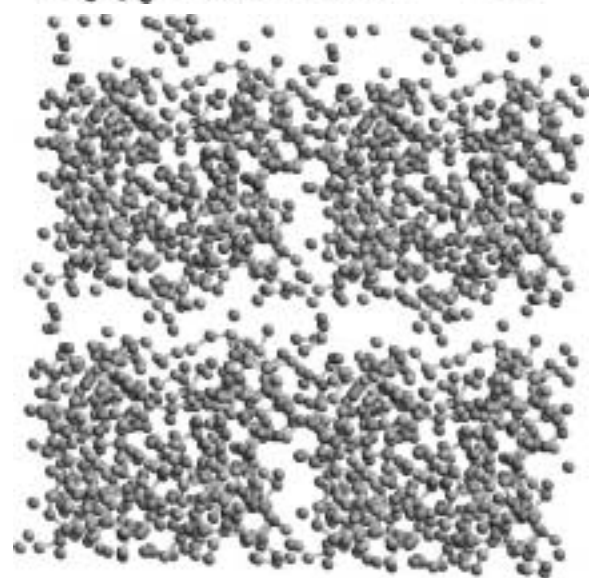
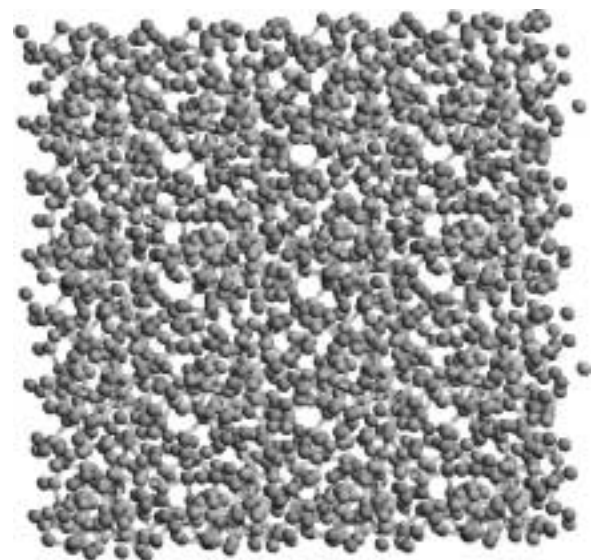


Figure 4 : Same as Fig. 3 except for the amorphous specimen.

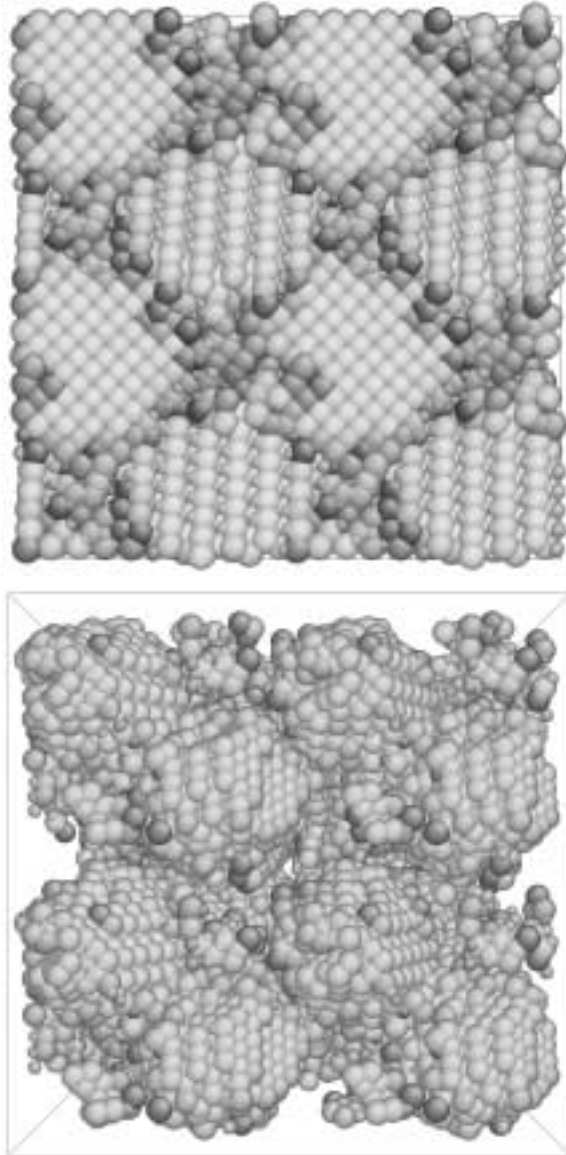


Figure 5 : Same as Fig. 3 except for the nanocrystal specimen.

to be intergranular decohesion. One can attempt to rationalize the characteristic behavior of the three types of responses in Fig. 2 through the effect of local disorder (or free volume), completely absent in the single crystal, well distributed in the amorphous phase, and localized at the grain boundaries in the nanocrystal. The disorder can act as a nucleation site for structural instability, and lowering the critical stress and strain for failure. Once a site is activated, it will tend to link up with neighboring activated sites, thus giving rise to different behavior between the amorphous and nanocrystal samples.

3 Toward Hall-Petch-Type Scaling

We have seen that microstructural features can have very dominant effects on strength and deformation. At present atomistic simulations of extended defect structures have been sufficiently well developed to treat the complex microstructures that exist in materials systems encountered in actual processing. For example, since high-strength SiC fibers have been produced in the laboratory, it would be desirable to have a method that allows the strength of a fiber specimen to be estimated given some reasonable characterization. As a first step toward such a goal, we will show how simulation results may be combined with simple concepts in fracture mechanics to deduce empirical scaling relations between strength and the size of dominant flaws in the microstructure, in the spirit of the Hall-Petch relation showing the strength of a polycrystalline material varying as inverse square root of the mean grain size.

Fig. 6 shows the variation of the ultimate tensile strength (UTS) of SiC with d , the “dominant flaw size”. We do not go into any detailed consideration of the physical origin of d other than saying that we expect the microstructure of every materials specimen should have such a characteristic size. The curve in Fig. 6 is obtained by noting another example of scaling, the variation of the critical stress required to propagate a cleavage crack with crack length d . From linear elastic fracture mechanics the Griffith expression for the critical stress intensity factor of a mode I crack is,

$$K_c^I = \sqrt{2\gamma E}, \quad (6)$$

where E is the Young’s modulus and γ the surface energy. We can compute K_c^I with values of E , γ determined using the Tersoff interatomic potential. Our values give a fracture toughness of $2.45 \text{ MPa} \cdot \text{m}^{1/2}$ for the

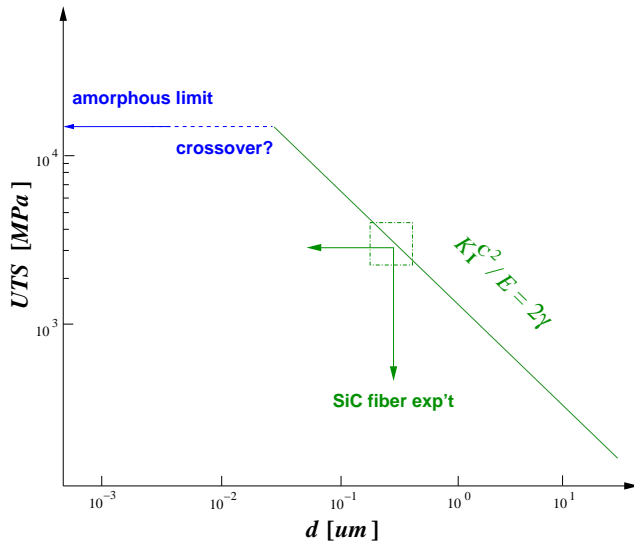


Figure 6 : Scaling behavior of ultimate tensile strength of SiC (3C) with size of dominant flaw showing limiting behavior approaching the amorphous phase.

$\langle 100 \rangle$ cleavage plane, in fair agreement with the experimental result of $2.8 \text{ MPa}\cdot\text{m}^{1/2}$ measured for sintered β -SiC polycrystal [Salvin and Quinn (1986)]. We then use $K_c^I = \sigma_c^\infty \sqrt{\pi d/2}$, or $\sigma_c^\infty = K_c^I / \sqrt{\pi d/2}$, where σ_c^∞ is the ultimate tensile stress and d , usually the crack length, now denotes the size of the dominant flaw. The curve in Fig. 6 thus has the same scaling dependence as the Hall-Petch relation. As a test of this correlation, we note for a controlling flaw size of .2 to .3 μm , Fig. 6 would predict a UTS of about 3 GPa. This turns out to be the strength measured in fine-diameter, high-strength, polymer-derived fibers which independent characterizations indicate to have such dominant flaw sizes. [Sacks (1999)].

In Fig. 6 we can make use of uniaxial tensile strength for nanocrystalline SiC determined in the same manner as Fig. 2. The dashed portion of the curve in Fig. 6 is only our conjecture for a crossover in the Hall-Petch relation [Nieh and Wadsworth (1991); Yip (1998)] based in part on the molecular dynamics results [Schiotz, Di Tolla, Jacobsen (1998)] pointing to an reverse Hall-Petch behavior obtained for an fcc metal Ni. It would be very interesting to map out this portion of Fig. 6. Except for a rough calculation suggesting that the critical grain size d_c for the crossover in a simple metal could be about 20 nm [Nieh and Wadsworth (1991)], we do not have any estimate of d_c . Simulation of mechanical behavior

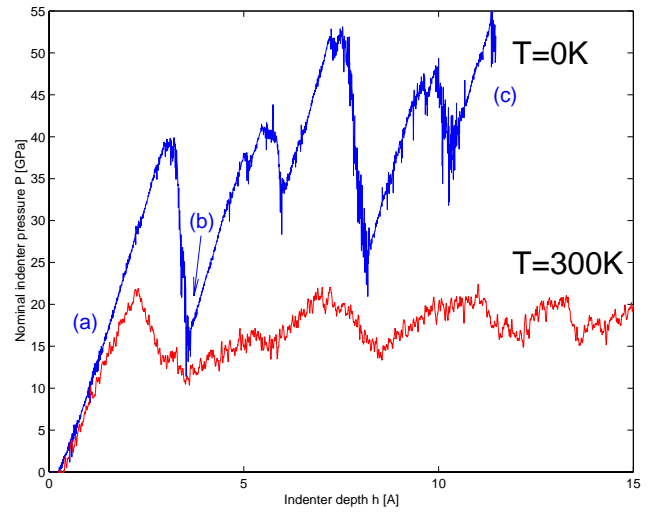


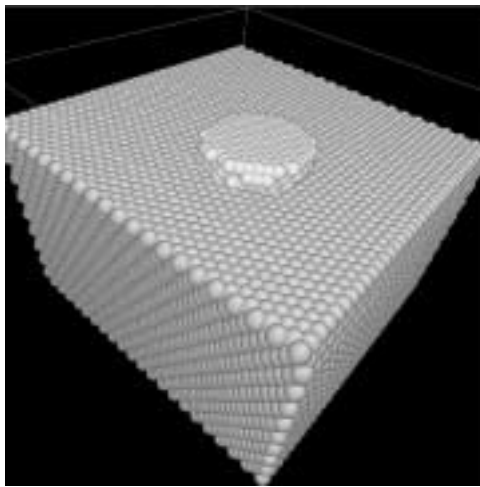
Figure 7 : Variation of nominal pressure response on a rigid indenter with indentation depth in a substrate of Cu thin film at 0K and 300K. Specific stages of indentation are indicated as (a), (b), and (c) (see Fig. 8).

of nanocrystals, like the study of theoretical strength of materials, would be timely because one can uniquely separate the effects of defects and impurities from the intrinsic behavior of the crystalline phase.

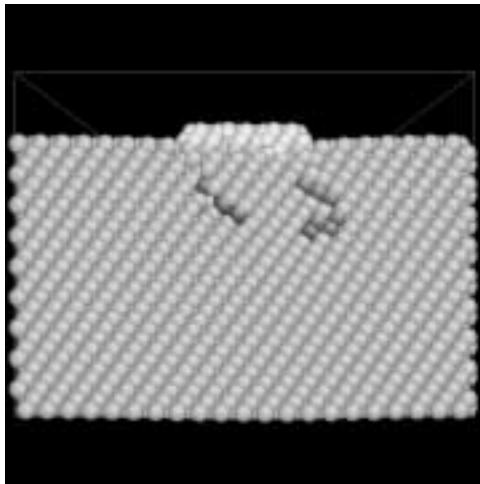
4 Nano-Indentation on Cu

We will briefly consider a recent molecular dynamics simulation of nano-indentation on Cu thin film using simulation cell of size $9.3 \times 7.0 \times 9.2 \text{ nm}$ (41,200 atoms) with periodic conditions [Li (2000)]. The (111) surface of the system faces the indenter, which is a rigid cylinder 2.5 nm in diameter, composed of immobile Cu atoms. Simulations are carried out at 0K and 300K using a many-body potential model [Rasmussen, Jacobsen, Leffers, Pederson (1997)]. The indenter is lowered onto the substrate in continuous increments of prescribed indenter depth. At each step, the substrate is allowed to relax and the nominal pressure, defined to be the total force on the indenter's immobile atoms exerted by all the substrate atoms divided by the indenter cross section (about 5 nm^2), is calculated. To compensate for the reaction force, the center of mass of all the mobile atoms is kept fixed. Temperature rescaling is applied to the entire system at each step to absorb the heat generated.

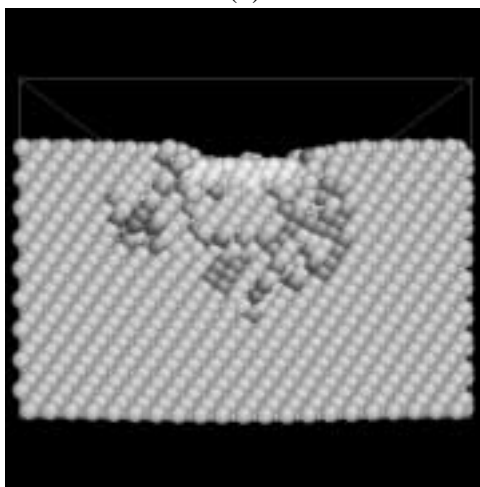
Fig. 7 shows the variation of the nominal pressure on the indenter with indenter depth h . At 0K one sees the pres-



(a)



(b)



(c)

Figure 8 : Side view of atomic configurations of a nano-indenter pushing into a substrate of Cu thin film, (a) initial setup, (b) at the first cusp in Fig. 7, and (c) after several cusps.

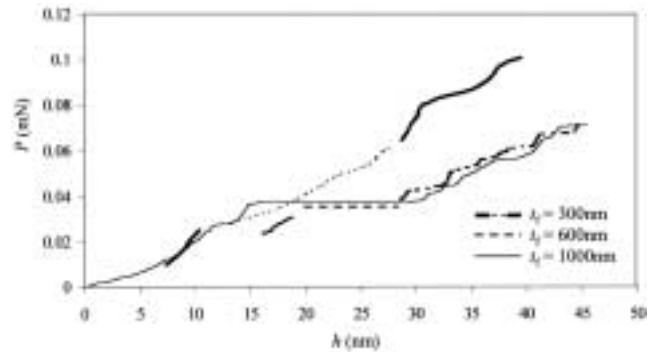


Figure 9 : Trace of indenter force versus indentation depth from experiment on polycrystalline Cu thin films [Fig. 8 of [Gouldstone, Koh, Zeng, Giannakopoulos, Suresh (2000)]; indenter $R = 50$ nm] showing intermittent bursts of dislocation emission.

sure rises and falls sharply; similar but less pronounced behavior is seen at 300K. There is an indication of apparent “hardening” at the low temperature, but not at the higher temperature. Fig. 8 shows the atomic configurations at three instants during the indentation run, initial position, immediately after the first cusp (labeled as (b)) in Fig. 7, and after several cusps (labeled (c)). One sees that the first cusp occurs at a nominal pressure of about 40 GPa (Fig. 7) with corresponding atomic configuration showing the nucleation of a dislocation loop with an edge-type Burgers vector (Fig. 8). After several cusps, the dislocation loops have moved away from the indenter, a pile-up effect has probably set in because of the small system size. It appears that several slip systems have been activated.

The simulation results may be compared with recent measurements of variation of indenter force with indenter depth h as shown in Fig. 9 [Gouldstone, Koh, Zeng, Giannakopoulos, Suresh (2000)]. One sees two types of responses, an elastic component associated with the monotonic rise of force with increasing, and a plastic component represented by a plateau region indicating large indentation, or dislocation burst, at no increase in force. This behavior has been interpreted as “intermittent plasticity”. In particular, the first burst of dislocation is believed to occur around the ideal shear strength of Cu, of around 15 GPa [Gouldstone, Koh, Zeng, Giannakopoulos, Suresh (2000)]².

²This value, predicted using linear elasticity solution under the indenter, is much higher than the recent *ab initio* calculation result

We believe there is correspondence between experiment and simulation in the periodic nucleation of dislocation loops, the first emission indeed occurring at stresses approaching the ideal shear strength. On the other hand, the fact that simulation takes place on such short time interval relative to experiment, along with the small system size, means that the nucleated dislocations effectively have no time to migrate away from the indenter. In effect, the pile up in the immediate vicinity of the indenter is likely the reason for the 'hardening' that is seen at 0K in simulation.

5 An Outlook on Multiscale Simulation

Given the theme of this Symposium is multiscale simulation of mechanics of materials, we conclude our discussion with a comment on the issue of linking atomistic simulations with mesoscale techniques in the context of materials strength. The integration of atomistic and mesoscale methods of simulation is absolutely essential for a systematic understanding of strength degradation in the presence of defect microstructure; currently this is a bottleneck with no generally satisfactory solution. Without going to length scale of micron and time scale of seconds, one will not be able to take into proper account the relevant microstructural deformations in order to achieve the correct strength determination. To bridge the length scales, the embedding of a molecular dynamics region with a finite-element surrounding continues to be an appealing notion; however, we still do not have much experience in coupling the two regions effectively without incurring unphysical effects [Cai, de Koning, Bulatov, Yip (2000)].

To bridge the time scales, the linking of atomistics with kinetic Monte Carlo could be a useful approach as suggested by a recent study of dislocation mobility in silicon [Cai Bulatov, Justo, Argon, Yip (2000)]. Here too, more applications are needed before we know how best to incorporate activation energies obtained by atomistics into a coarse-grained simulation without the atoms. In each case a basic challenge is to provide sufficient degrees of freedom for the defect microstructure to respond to an external loading in a natural manner, and to understand the connection between local driving force for defect mobility and the external loading [Li (2000)]. We plan to address this issue and show preliminary results in

the months ahead.

Acknowledgement: This work was supported by the Air Force Office of Scientific Research (Grant F49620-00-10082) and the National Science Foundation (DMR-9980015). SY also acknowledges support by an ASCI-Level 2 grant from the Lawrence Livermore National Laboratory.

Reference

Report of the National Workshop on Advanced Scientific Computing, July 30-31, 1998 (National Academy of Sciences). Copies of the report may be obtained from:

<http://www.sc.doe.gov/ascr/mics/archive.html>

Special Issue of *J. Computer-Aided Mater. Design*, vol. 3, (1996); special issue of *Current Opinion in Solid State and Mater. Sci.*, vol. 3, no. 6 (1998).

Campbell, G. H.; Foiles, S. M.; Huang, H.; Hughes D. A.; King W. E.; Lassila D. H.; Nikkel D. J.; de la Rubia T. D.; Shu J. Y.; Smyshlyaev V. P. (1998): Multi-scale modeling of polycrystal plasticity: a workshop report. *Materials Science & Engineering A*, vol. 251, pp. 1-22.

Born, M. (1940): *Proc. Cambridge Philos. Soc.*, vol. 36, pp. 160.

Born, M.; Huang, K. (1956): *Dynamical Theory of Crystal Lattices*, Clarendon, Oxford.

Hill, R. (1975): On the elasticity and stability of perfect crystals at finite strain. *Mathematical Proceedings of the Cambridge Philosophical Society*, vol. 77, pp. 225-40.

Hill, R. and Milstein, F. (1977): Principles of stability analysis of ideal crystals. *Phys. Rev. B*, vol. 15, pp. 3087-96.

Kelly, A. and Macmillan, N. H. (1986): *Strong Solids*, 3rd ed., Clarendon, Oxford.

Wang, J.; Li, J.; Yip, S.; Phillpot, S.; Wolf, D. (1995): Mechanical instabilities of homogeneous crystals. *Phys. Rev. B*, vol. 52, pp. 12627-35.

Wallace, D. C. (1972): *Thermodynamics of Crystals*, Wiley, New York.

Zhou, Z.; Joos, B. (1996): Stability criteria for homogeneously stressed materials and the calculation of elastic constants. *Phys. Rev. B*, vol. 54, pp. 3841-50.

Morris, J. W. and Krenn, C. R. (2000): The internal

[Roundy, Krenn, Cohen, Morris (1999)] of 2.65 GPa for Cu.

- stability of an elastic solid. *Philos Mag. A*, vol. 80, pp. 2827-40.
- Barron, T. H. K.; Klein, M. L.** (1965): Second-order elastic constants of a solid under stress. *Proc. Phys. Soc.*, vol. 85, pp. 523-532.
- Hoover, W. G.; Holt A. C.; Squire D. R.** (1969): Adiabatic elastic constants for argon. Theory and Monte Carlo calculations. *Physica A*, vol. 44, pp. 437-43.
- Basinski, Z. S.; Duesbery M. S.; Pogany A. P.; Taylor R.; Varshni Y. P.** (1970): An effective ion-ion potential for sodium. *Canadian Journal of Physics*, vol. 48, pp. 1480-9.
- Wang, J.; Yip, S.; Phillpot, S.; Wolf, D.** (1993): Crystal instabilities at finite strain. *Phys. Rev. Lett.*, vol. 71, pp. 4182-5.
- Mizushima, K.; Yip, S.; Kaxiras, E.** (1994): Ideal crystal stability and pressure-induced phase transition in silicon. *Phys. Rev. B*, vol. 50, pp. 14952-9.
- Tang, M. and Yip, S.** (1994): Lattice instability in β -SiC and simulation of brittle fracture. *J. Appl. Phys.*, vol. 76, pp. 2719-2725.
- Cleri, F.; Wang, J.; Yip, S.** (1995): Lattice instability analysis of a prototype intermetallic system under stress. *J. Appl. Phys.*, vol. 77, pp. 1449-58.
- Tang, M. and Yip, S.** (1995): Atomic size effects in pressure-induced amorphization of a binary covalent lattice. *Phys. Rev. Lett.*, vol. 75, pp. 2738-41.
- Tersoff, J.** (1989): Modeling solid-state chemistry: interatomic potentials for multicomponent systems. *Phys. Rev. B*, vol. 39, pp. 5566-8.
- Li, J.** (2000): Ph.D. Thesis, Department of Nuclear Engineering, Massachusetts Institute of Technology.
- Galli, G.; Gygi, F.; Catellani, A.** (1999): Quantum Mechanical Simulations of Microfracture in a Complex Material. *Phys. Rev. Lett.*, vol. 82, pp. 3476-9.
- Sacks, M. D.** (1999): Effect of composition and heat treatment conditions on the tensile strength and creep resistance of SiC-based fibers. *Journal of the European Ceramic Society*, vol. 19, pp. 2305-15.
- Nieh, T. G.; Wadsworth, J.** (1991): Hall-Petch relation in nanocrystalline solids. *Scripta Metallurgica et Materialia*, vol. 25, pp. 955-8.
- Yip, S.** (1998): Nanocrystals - the strongest size. *Nature*, vol. 391, pp. 532-533.
- Schiotz, J.; Di Tolla, F. D.; Jacobsen, K. W.** (1998): Softening of nanocrystalline metals at very small grain sizes. *Nature*, vol. 391, pp. 561-3.
- Rasmussen, T.; Jacobsen, K. W.; Leffers, T.; Pederson, O. B.** (1997): Simulations of the atomic structure, energetics, and cross slip of screw dislocations in copper. *Phys. Rev. B*, vol. 56, pp. 2977-90.
- Romano, A.; Li, J.; Yip, S.** (2002): Atomistic simulation of matter under stress: crossover from hard to soft materials. *Physica A* 304 (2002) 11-22.
- Gouldstone, A.; Koh, H.-J.; Zeng, K.-Y.; Giannakopoulos, A. E.; Suresh, S.** (2000): Discrete and continuous deformation during nanoindentation of thin films. *Acta Materialia*, vol. 48, pp. 2277-2295.
- Cai, W.; de Koning, M.; Bulatov, V.; Yip, S.** (2000): Minimizing boundary reflections in coupled-domain simulations. *Phys. Rev. Lett.*, vol. 85, pp. 3213-16.
- Cai, W.; Bulatov, V. V.; Justo, J. F.; Argon, A. S.; Yip, S.** (2000): Intrinsic mobility of a dissociated dislocation in silicon. *Phys. Rev. Lett.*, vol. 84, pp. 3346-9.
- Slavin, M. J.; Quinn, G. D.** (1986): Mechanical property evaluation at elevated temperature of sintered β -silicon carbide. *International Journal of High Technology Ceramics*, vol. 2, pp. 47-63.
- Roundy, D.; Krenn, C. R.; Cohen, M. L.; Morris J. W.** (1999): Ideal shear strengths of FCC aluminum and copper. *Phys. Rev. Lett.*, vol. 82, pp. 2713-2716.

